

The response of wildfire regimes to Last Glacial Maximum carbon dioxide and climate

Olivia Haas^{1,2}, Iain Colin Prentice^{1,2}, Sandy P. Harrison^{1,3}

¹Leverhulme Centre for Wildfires, Environment and Society, Imperial College London, South Kensington, London SW7 2BW, UK

²Georgina Mace Centre for the Living Planet, Department of Life Sciences, Imperial College London, Silwood Park Campus, Buckhurst Road, Ascot SL5 7PY, UK

³Geography & Environmental Science, University of Reading, Whiteknights, Reading RG6 6AH, UK

Correspondence to: Olivia Haas (o.haas20@imperial.ac.uk)

Abstract

Climate and fuel availability jointly control the incidence of wildfires. The effects of atmospheric CO₂ on plant growth influence fuel availability independently of climate; but the relative importance of each in driving large-scale changes in wildfire regimes cannot easily be quantified from observations alone. Here, we use previously developed empirical models to simulate the global spatial pattern of burnt area, fire size and fire intensity for modern and Last Glacial Maximum (LGM; ~ 21,000 ka) conditions using both realistic changes in climate and CO₂ and sensitivity experiments to separate their effects. Three different LGM scenarios are used to represent the range of modelled LGM climates. We show large, modelled reductions in burnt area at the LGM compared to the recent period, consistent with the sedimentary charcoal record. This reduction was predominantly driven by the effect of low CO₂ on vegetation productivity. The amplitude of the reduction under low CO₂ conditions was similar regardless of the LGM climate scenario and was not observed in any LGM scenario when only climate effects were considered, with one LGM climate scenario showing increased burning under these conditions. Fire intensity showed a similar sensitivity to CO₂ across different climates but was also sensitive to changes in vapour pressure deficit (VPD). Modelled fire size was reduced under LGM CO₂ in many regions but increased under LGM climates because of changes in wind strength, dryness (DD) and diurnal temperature range (DTR). This increase was offset under the coldest LGM climate in the northern latitudes because of a large reduction in VPD. These results emphasise the fact that the relative magnitudes of changes in different climate variables influence the wildfire regime and that different aspects of climate change can have opposing effects. The importance of CO₂ effects imply that future projections of wildfire must take rising CO₂ into account.

1. Introduction

Climate influences the occurrence of wildfires both through fire weather, which affects the probability of wildfire start and spread, and the long-term establishment of vegetation which is strongly controlled by temperature and precipitation (Bradstock, 2010; Pausas & Ribeiro, 2013). It has been suggested that current climate change, driven by increasing atmospheric CO₂ levels, will increase wildfire risk in many regions through increased fuel dryness whilst potentially reducing wildfire risk in some regions due to decreasing fuel availability (e.g. Abatzoglou et al., 2019a; Bowman et al., 2020; Harrison et al., 2021; Rogers et al., 2020). However,

36 atmospheric CO₂ levels also affect fuel loads independently of climate through physiological effects on
37 photosynthesis which cascade into plant growth rates (Bond et al., 2003; Bond & Midgley, 2012; Kgope et al.,
38 2010). Much emphasis has been placed on recent and future changes in fire weather (see e.g. Abatzoglou et al.,
39 2019; Betts et al., 2015; Flannigan et al., 2013; Jolly et al., 2015). However, increases in atmospheric CO₂
40 concentrations promote vegetation productivity, thus altering fuel availability and loads, as well as affecting fuel
41 types through e.g. woody thickening (Buitenwerf et al., 2012; Donohue et al., 2013; Knorr et al., 2016; Martin
42 Calvo et al., 2014; Martin Calvo & Prentice, 2015; Pausas, 2015). Fuel properties have different effects on
43 different aspects of the fire regime, with fire size strongly constrained by fuel continuity and fire intensity limited
44 by fuel loads (Archibald et al., 2013; Haas et al., 2022). Thus, CO₂-induced changes in vegetation properties will
45 most likely affect these aspects of wildfire regimes differently.

46 One reason the impact of CO₂ on wildfires is poorly constrained is the difficulty of isolating it based on
47 observations alone. Satellite records only span ~25 years, a relatively short period to monitor the effect of changing
48 CO₂ levels on the vegetation properties that influence wildfires. Furthermore, changes in atmospheric CO₂ levels
49 and climate are temporally correlated, and since both affect vegetation, it difficult to attribute changes in
50 observations to one or the other. An alternative approach is to use process-based fire-enabled vegetation models
51 which explicitly account for the physiological effects of CO₂ and can be used to examine the temporal and spatial
52 patterns of wildfires under different conditions. Process-based models have been used to examine the impact of
53 climate and atmospheric CO₂ changes on both vegetation and wildfire at the last glacial maximum (LGM; 21,000
54 years ago) (Martin Calvo et al., 2014; Martin Calvo & Prentice, 2015). The LGM is a useful out-of-sample
55 experiment since the climate forcing is of similar magnitude as the change expected by the end of the century in
56 high-end scenarios, though of opposite sign (Kageyama et al., 2021). The LGM had a generally colder and drier
57 climate than today, with CO₂ levels ~ 185 ppm. Palaeorecords show reduced vegetation productivity and forest
58 cover (Harrison & Prentice, 2003; Kaplan et al., 2016; Moreno et al., 2018), and ice core and sedimentary charcoal
59 records indicate reduced biomass burning globally (Albani et al., 2018; Harrison et al., 2022; Marlon et al., 2016;
60 Rubino et al., 2016). Although this reduction could reflect the colder and drier conditions, model experiments
61 suggests that low CO₂ also played a crucial role. Experiments using the coupled biogeography and
62 biogeochemistry model BIOME4 (Kaplan et al., 2003) showed that it was necessary to include the direct effect
63 of CO₂ to simulate observed global and regional reduction in forest cover during the glacial (Bragg et al., 2013;
64 Harrison & Prentice, 2003). Similarly, Martin Calvo et al. (2015) showed that low CO₂ was necessary to simulate
65 the observed reduction of biomass burning in LGM experiments using the LPX fire-enabled vegetation model.

66 In this analysis, we use three empirical models (Haas et al., 2022) to explore the relative importance of
67 climate and of CO₂ on the global spatial patterns of burnt area, fire size and fire intensity. We performed two
68 experiments under realistic modern CO₂ and climate conditions (MOD climate/MOD CO₂ and LGM
69 climate/LGM CO₂). We also performed two counterfactual sensitivity experiments to quantify the sensitivity of
70 each wildfire property to climate and CO₂ independently (MOD climate/LGM CO₂ and LGM climate/MOD CO₂).
71 Comparisons to LGM charcoal records from the Reading Palaeofire Database (RPD) (Harrison et al., 2022) were
72 used to examine which experiments provided the most realistic spatial patterns.

2. Methods

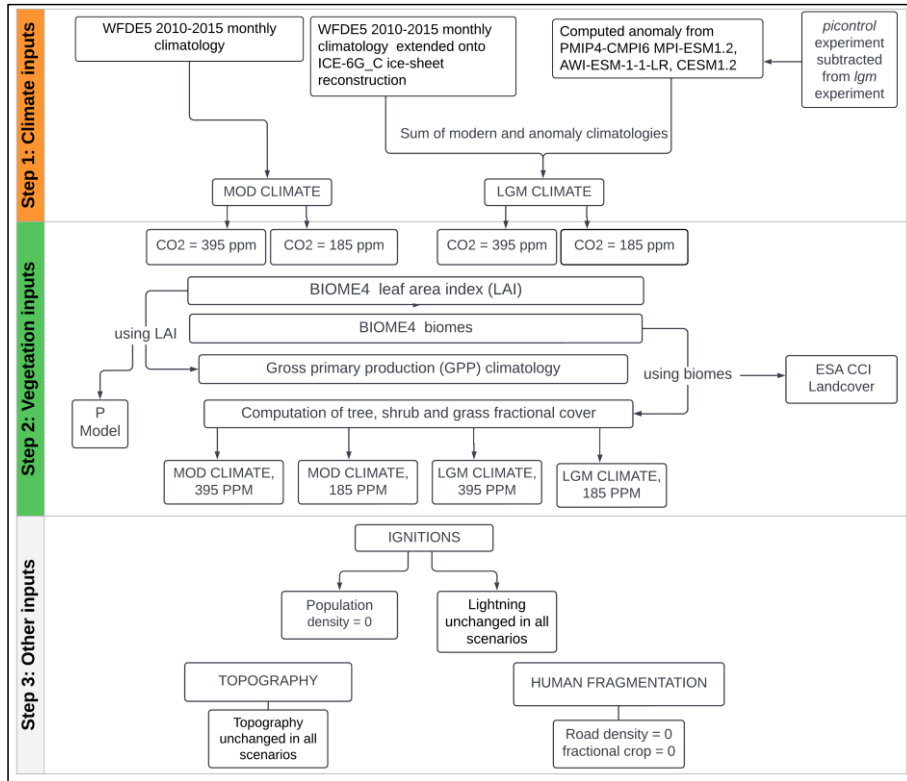


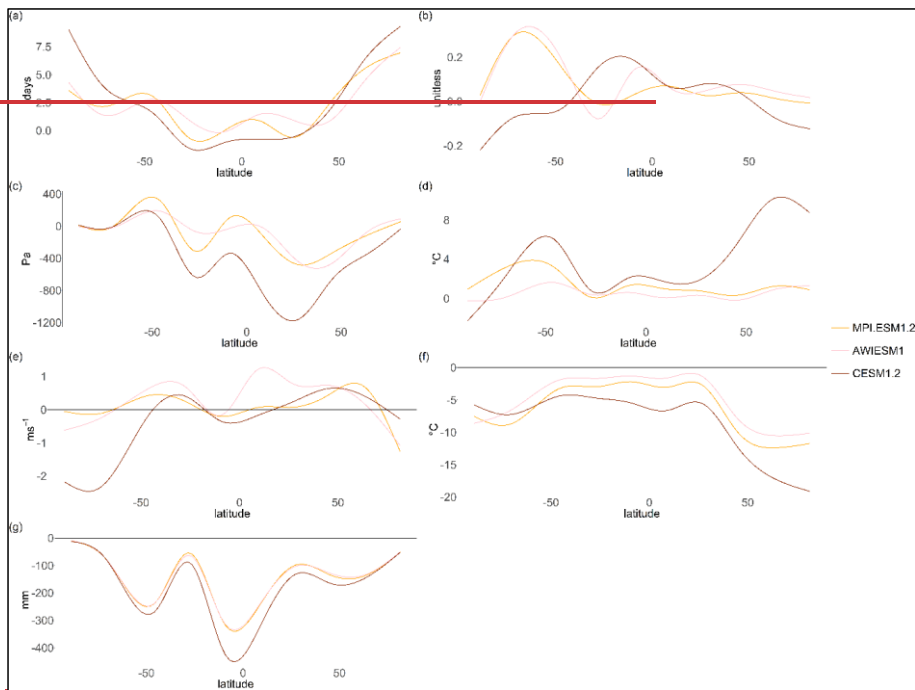
Figure 1. Flowchart of the method to obtain each of the four scenarios: MOD climate and MOD CO₂, LGM climate and LGM CO₂, MOD climate and LGM CO₂ and LGM climate and LGM CO₂.

Haas et al (2002) developed empirical models of the global spatial patterns of burnt area (BA), fire size (FS) and fire intensity (FI) using generalised linear modelling (GLM) of modern observations. Here we use these models to simulate the global spatial patterns of burnt area (BA), fire size (FS) and fire intensity (FI) under four climate/CO₂ scenarios (Figure 1). The empirical models were developed by applying generalised linear modelling (GLM) to modern observations (Haas et al., 2022) to simulate the global spatial patterns of burnt area (BA), fire size (FS) and fire intensity (FI) under four climate/CO₂ scenarios (Figure 1). We used two realistic scenarios: (a) MOD climate and CO₂ conditions and (b) LGM climate and CO₂. We ran two sensitivity experiments (a) combining MOD climate and LGM CO₂ and (b) combining LGM climate and MOD CO₂ levels. The empirical models use climate, vegetation, topography, lightning ignitions, land cover, road density and human population density as predictors to represent the environmental controls on each of the wildfire properties.

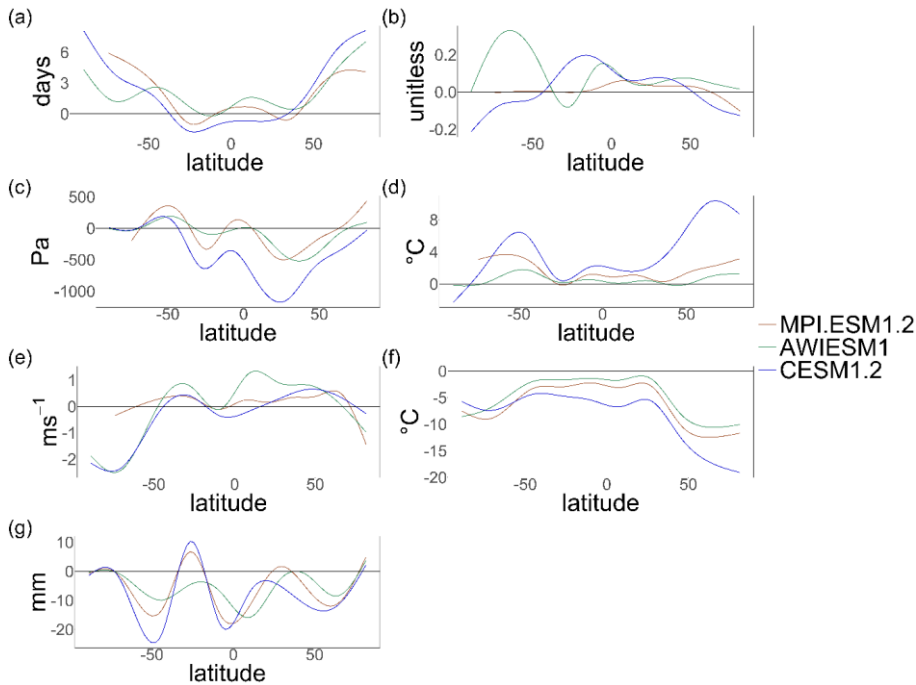
Modern (MOD) climate data (daily temperature (T), daily precipitation (P), photosynthetic photon flux density (PPFD), monthly wind speeds (wind), vapour pressure deficit (VPD), monthly specific humidity (huss), cloud cover (cld), monthly pressure (Pa)) were obtained from the WFDE5 bias-adjusted ERA5 database (Cucchi

91 et al., 2020) for 2010 to 2015. The number of monthly dry days (DD) (days with ≤ 1 mm of precipitation), monthly
 92 diurnal temperature range (DTR) (daily maximum temperature – daily minimum temperature) and monthly
 93 vapour pressure deficit (VPD), a function of specific humidity, temperature and pressure were all calculated
 94 following the methodology in Haas et al. (2022). Following the methodology in Haas et al. (2022), the number of
 95 monthly dry days (DD) and monthly diurnal temperature range (DTR) were calculated. Seasonal climatologies
 96 were derived for all variables eliminating inter-annual variability. For each grid cell, values from the month with
 97 (on average) the maximum number of DD, the largest DTR, and the highest VPD were selected. Wind speed value
 98 was taken from the hottest month of the year (determined from the WFDE5 2 m air temperature (Cucchi et al.,
 99 2020)). For lightning, the mean value over the seasonal climatology was selected. A seasonality predictor to
 100 account for wet vs dry seasons was constructed by dividing the range of monthly values from the seasonal DD
 101 climatology by the mean value of all 12 months. Expanded ice sheets in North America, Fennoscandia, Greenland,
 102 and Antarctica resulted in global sea levels ~ 120 m lower than today at the LGM. The modern climate data
 103 were extrapolated out onto the exposed shelves using the ICE-6G_C (Peltier et al., 2015) boundary conditions and
 104 a nearest neighbour approach from the *GeoInterpolation* package in R.

105



106



107
108

109 **Figure 2.** Latitudinal distribution of the LGM-MOD climate anomalies for MPI.ESM1.2 (orange), AWI-
 110 ESM1.2 (pink) and CESM1.2 (brown) for (a) the maximum number of dry days, (b) the seasonality of dry days,
 111 (c) maximum monthly VPD, (d) maximum monthly DTR, (e) maximum monthly mean wind speeds, (f) mean
 112 monthly temperature and (g) mean monthly total precipitation. The zero-intercept line represents no change
 113 between LGM and MOD climate, with negative values representing lower values at the LGM and positive
 114 values representing higher values at the LGM.

115

116 LGM climate data were obtained from three models participating in the Palaeoclimate Modelling
 117 Intercomparison Project (PMIP) contribution to the sixth phase of the Coupled Model Intercomparison Project
 118 (CMIP6), AWI-ESM-1-1-LR (short name: AWIESM1) (Lohmann et al., 2020; Sidorenko et al., 2015),
 119 MPI_ESM1.2 (Mauritsen et al., 2019), CESM1.2 (F. Li et al., 2013; Tierney et al., 2020) to represent a range of
 120 LGM climates (Figure 2). A seasonal climatology was derived for each climate variable from the PMIP *picontrol*
 121 experiment (pre-industrial conditions, PI) and the PMIP *Igm* experiment of the PMIP4-CMIP6 simulations. The
 122 difference between the PI and LGM values (LGM-PI climate anomalies) were calculated and added to the MOD
 123 climatology (LGM-MOD climate anomalies) (see Figure 1). We use the term climate anomalies to refer to the
 124 difference between the MOD climatology for each climate variable and the computed bias-adjusted LGM
 125 climatology for the same variable, consistent with the PMIP4 protocol (Kageyama et al., 2017). The use of
 126 anomalies is designed to minimise the impact of systematic model biases on the derived climate. This approach
 127 provided three LGM climate scenarios, resulting in twelve experiments for BA, FS and FI respectively.

128 between the PI and LGM values (LGM-PI climate anomalies) were calculated and added to the MOD climatology
 129 (LGM-MOD climate anomalies) (see Figure 1). The use of anomalies is designed to minimise the impact of
 130 systematic model biases on the derived climate. This approach provided three LGM climate scenarios, resulting
 131 in nine experiments for BA, FS and FI respectively.

132
 133 We obtained MOD and LGM vegetation and gross primary production (GPP) using the coupled
 134 biogeography and biogeochemistry model BIOME4 (Kaplan et al., 2003) and a simple optimality-based model of
 135 GPP, the P Model (Wang et al., 2017; Stocker et al., 2020). BIOME4 was used to simulate biome distribution
 136 with modern day climate data (T, P, cld) setting CO₂ levels to 395 ppm (the annual mean from 2010-2015) and
 137 185 ppm in turn. LGM biome distributions were simulated using the three different LGM scenarios, again setting
 138 CO₂ levels to 395 ppm and 185 ppm respectively. We derived mean fractional tree, shrub, and grass cover for
 139 each of these nine-twelve experiments using the mean values for each biome from ESA CCI Landcover (W. Li et
 140 al., 2018). We also calculated fAPAR for each experiment from the leaf area index (LAI) computed by BIOME4
 141 and obtained fractional cover of C₄ plants (see S1). We computed global monthly C₃ and C₄ photosynthesis using
 142 the P model using appropriate combinations of climate (T, VPD, ppfd and Pa), BIOME4-derived fAPAR and CO₂
 143 concentration for the MOD and LGM scenarios (see Figure 1). Total GPP was calculated as:

$$GPP_{monthly} = GPP_{c3}(1 - C4_{fraction}) + GPP_{c4}C4_{fraction} , \quad (1)$$

144 with GPP_{c3} and GPP_{c4} representing monthly C₃ and C₄ GPP values from the P Model and $C4_{fraction}$ representing
 145 the fractional C₄ cover from BIOME4 (see Table1).

Scenario	Modern climate	MPI_ESM1.2	AWIESM1	CESM1.2 LGM
Modern CO ₂ (395 ppm)	149.37	106.63	112.06	88.44
LGM CO ₂ (185 ppm)	66.54	55.49	69.61	50.37

148
 149 **Table 1.** Total annual gross primary production (GPP) (in PgC) estimates for each scenario.

150
 151 This approach led to estimates of total BA, median FS, and median FI under modern conditions of a similar
 152 magnitude to the original GLM models and other global estimates (Andela et al., 2019; Humber et al., 2019)
 153 (Table 2).

154 Topographic and lightning variables were assumed not to change dramatically-between the LGM and the
 155 present day. We used modern values, extrapolated out onto the exposed shelves, for the LGM experiments. The
 156 GLMs (Haas et al., 2022) include predictors associated with human activity, specifically human population
 157 density, road density and cropland cover. Population density is used as a measure of potential human ignitions
 158 and road density and cropland cover as measures of landscape fragmentation. Including these anthropogenic
 159 predictors in the GLM models was found to be essential to capture the global drivers of the observed spatial
 160 patterns of wildfires (Haas et al., 2022). This is because modern fire regimes are influenced by human activity at
 161 a global scale (e.g. Marlon et al., 2008; Bowman et al., 2020; Harrison et al., 2021). However, although the practice
 162 of foraging for plants by some hunter-gatherer communities at the LGM has been shown (Liu et al., 2013), we
 163 presume that there was no large-scale agriculture (or road networks) at the LGM. Additionally, information about
 164 pre-agricultural population sizes is limited and highly uncertain (see e.g. Williams et al., 2013; Gautney &

165 [Holliday, 2015](#)) and though some regional models of human population do exist ([Tallavaara et al., 2015](#)), a reliable
166 [global product is not yet available. To avoid confounding effects due to the high uncertainty of human impacts on](#)
167 [global wildfire regimes, we decided to exclude these anthropogenic predictors in all the experiments by setting](#)
168 [them to zero. This ensured that differences between the experiments were driven solely by climate and CO₂. We](#)
169 [performed sensitivity analysis to examine the impact of setting human predictors to zero under modern and LGM](#)
170 [conditions \(see S2\). Whilst BA and FS increase in the modern sensitivity analyses \(especially in areas with high](#)
171 [road density and cropland density such as Europe and India\) the effect was negligible for FI, highlighting the](#)
172 [sensitivity of BA and FS to human activity. Under LGM conditions, the effect of including human population was](#)
173 [negligible for all three fire properties. This reflects the slight and localised human impact on the natural landscape](#)
174 [at the LGM \(\[Black et al, 2007\]\(#\); \[Fuller et al., 2014\]\(#\); \[Portenga et al., 2016\]\(#\)\). The original GLM models \(\[Haas et al.,\]\(#\)](#)
175 [2022\) included predictors associated with human activity, specifically road density, cropland cover and population](#)
176 [density. However, since there was no agriculture at the LGM and the human impact on the natural landscape was](#)
177 [slight and relatively localised \(\[Fuller et al., 2014\]\(#\)\), we excluded these predictors in all the experiments by setting](#)
178 [them to 0. This also ensured observed differences between the experiments were driven solely by climate and](#)
179 [CO₂. Exclusion of predictors related to human activity increases BA and FS in the original GLM models and](#)
180 [produces an even larger increase when changes in vegetation are considered through using the BIOME4 derived](#)
181 [vegetation \(Table 2\). The effect was negligible for FI, highlighting the sensitivity of BA and FS to human activity.](#)
182

Inputs for land cover and P Model GPP (Cocchi et al., 2020)	ESA — CCI Landcover NASA/GIMS fAPAR 3g	BIOME4 (Kaplan et al., 2003)	Global estimates from the literature
Burnt area (millions km²)			
<i>Human activity on</i>	4.42	4.25	[1.87–4.6] (Humber et al., 2019)
<i>Human activity off</i>	7.41	11.27	
Fire size (km²)			
<i>Human activity on</i>	3.36	3.61	4.4 (Andela et al., 2019) (does not include wildfires smaller than 0.21 km ²)
<i>Human activity off</i>	5.34	6.25	
Fire intensity (W.km⁻¹)			
<i>Human activity on</i>	40.00	31.41	
<i>Human activity off</i>	39.20	31.17	

183
184 **Table 2.** Sensitivity of GLM models to human activity using both observations and BIOME4 derived
185 vegetation and GPP.
186

187 When modelled GPP values were 0, BA, FS and FI was automatically set to 0. Modelled BA values smaller
188 than 0.001 were assumed to imply no burning, thus under these conditions FS and FI were also assumed to be 0
189 since both GLM models were trained on data of existing fires (see [S32](#)).

190 The resulting BA, FS and FI anomalies refer to the difference between the MOD climate/MOD CO2
191 experiment and the three other experiments since each experiment is considered to represent the long-term average
192 spatial pattern for each fire property under the set experimental conditions. We used the sensitivity experiments
193 to quantify the separate effects of CO2 and climate on BA, FS and FI independently. We then used the realistic
194 experiments to identify which predictors were driving the largest change between MOD and the three LGM
195 scenarios by excluding one predictor at a time from the GLM models, re-running the LGM experiments and
196 identifying which excluded variable caused the greatest change in the BA, FS and FI MOD-LGM anomalies in
197 each grid-cell. Comparing these results to the BA, FS and FI MOD-LGM anomalies of the full GLM models
198 allowed us to determine if the predictor was responsible for an increase or a decrease in BA, FS and FI. We then
199 used the realistic experiments to identify which predictors were driving the largest change between MOD and the
200 three LGM scenarios by excluding one predictor at a time from the GLM models, re-running the LGM
201 experiments and identifying which excluded variable caused the greatest change in the BA, FS and FI MOD-LGM
202 anomalies in each grid-cell. Comparing these results to the BA, FS and FI MOD-LGM anomalies of the full GLM
203 models allowed us to determine if the predictor was responsible for an increase or a decrease in BA, FS and FI.

204 We also compared the spatial patterns of BA, FS and FI with sedimentary charcoal data from the Reading
205 Palaeofire Database (RPD; Harrison et al., 2022). Sedimentary charcoal records provide a record of fire activity
206 but may reflect changes in both burnt area or completeness of combustion (Power et al., 2008) so this comparison
207 allowed us firstly to establish which of the fire regimes properties was most closely reflected in these records and
208 secondly which of the scenarios produced the most realistic patterns of burning. Model outputs and the charcoal
209 records were re-gridded to the coarsest resolution of the three climate models (2.5° x 1.875° resolution). We
210 calculated the number of correctly predicted BA, FS or FI anomalies (same sign within a given grid-cell),
211 separating positive and negative BA, FS or FI anomalies to assess the rate of false positives as well as false
212 negatives for each scenario and each LGM climate scenario.

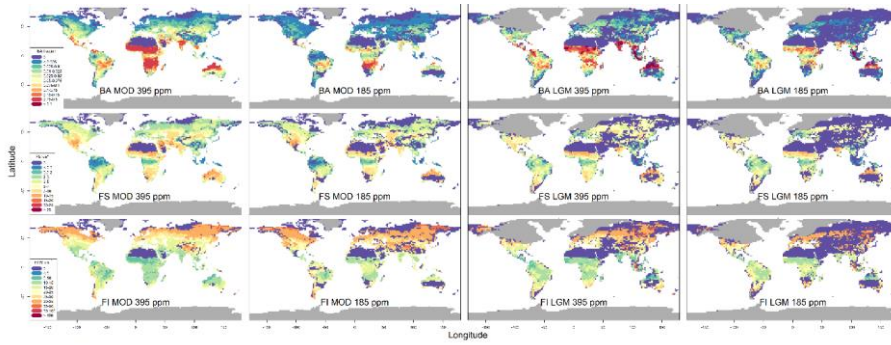
213 3. Results

214 Global BA was substantially reduced compared to the realistic MOD scenario under all three realistic
215 LGM scenarios, decreasing by 72% for the coldest CESM1.2 LGM scenario, 62% for the MPI-ESM1.2 LGM
216 scenario and 41% for the warmest AWIESM1 LGM scenario. The largest decreases were observed in sub-Saharan
217 Africa (excluding the tropical regions) as well as northern Australia and the Indian subcontinent (MPI-ESM1.2
218 and CESM1.2 LGM scenarios). Some increases in BA were observed in Alaska (MPI-ESM1.2 and AWIESM1
219 LGM scenarios) as well as south-East Asia, Indonesia, Papua-New-Guinea, and the northern tip of Australia.
220 Increases in Somalia and Central America were also observed (MPI-ESM1.2 and AWIESM1 LGM scenarios).
221 The number of grid cells (excluding ice covered cells) in which no burning occurred was 3 times higher in the
222 MPI-ESM1.2 and AWIESM1 LGM scenarios and 4 times higher in the CESM1.2 LGM scenario compared to the
223 realistic MOD scenario. This was driven by the expansion of desert and tundra biomes at the LGM. The Arabian
224 plate, Middle East, inland China and Australia, and the tips of South America and Africa saw burning reduced to
225 zero. Nearly all burning above 60°N was excluded, except for Alaska under the MPI-ESM1.2 and AWIESM1
226 LGM scenarios, with the exclusion extending down to 50°N for the CESM1.2 LGM scenario (see S3).

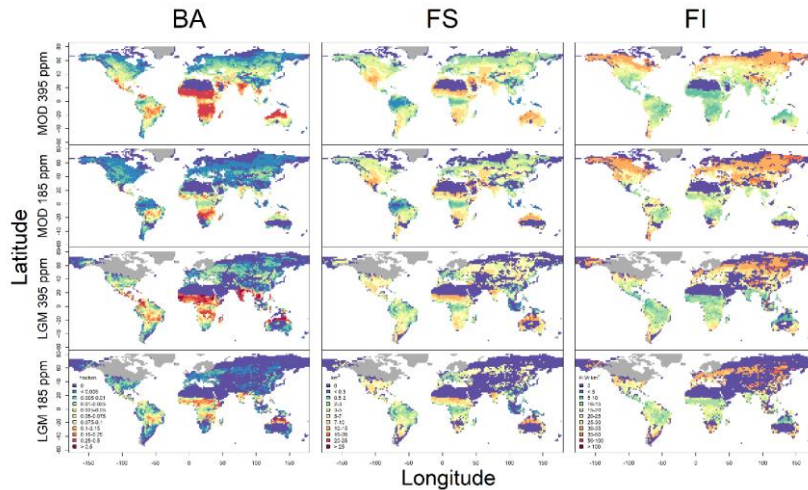
227 Globally, there was a large decrease in global median FS and FI when considering all grid-cells (not
228 covered in ice) because of overall global reduction in burning. Under all three LGM scenarios, global median FS

229 and FI were reduced to 0 compared to $\sim 5\text{km}^2$ for FS and 40W.km^2 for FI. However, when excluding grid-cells in
 230 which no burning occurred, both global median FS increased compared to the realistic MOD scenario (by $\sim 16\%$
 231 under the two less conservative scenarios (MPI-ESM1.2 and AWIESM1) and by 12% under the CESM1.2 LGM
 232 scenario). The main increases in FS occurred in the Central America, Amazonia, tropical Africa as well as the
 233 Indian Subcontinent and Europe and Asia between 30°N and 60°N (except for CESM1.2 which had very few
 234 positive FS anomalies). The largest reductions were observed North America, southern Australia, Middle East,
 235 and the rest of Eurasia. Global median FI also increased in regions that were burning under two of the LGM
 236 scenarios, by 11% under the CESM1.2 LGM scenario and by 4% for MPI.ESM1.2 LGM scenario. Under the
 237 AWIESM1 LGM scenario global median FI decreased by 2% even when excluding grid-cells that were not
 238 burning. Despite this, changes in FI were spatially consistent across all three LGM scenarios, with increases in FI
 239 occurring primarily across the American and African continents, as well as the Mediterranean Basin and Europe
 240 and decreases occurring in Asia and inland Australia.

241



242



243

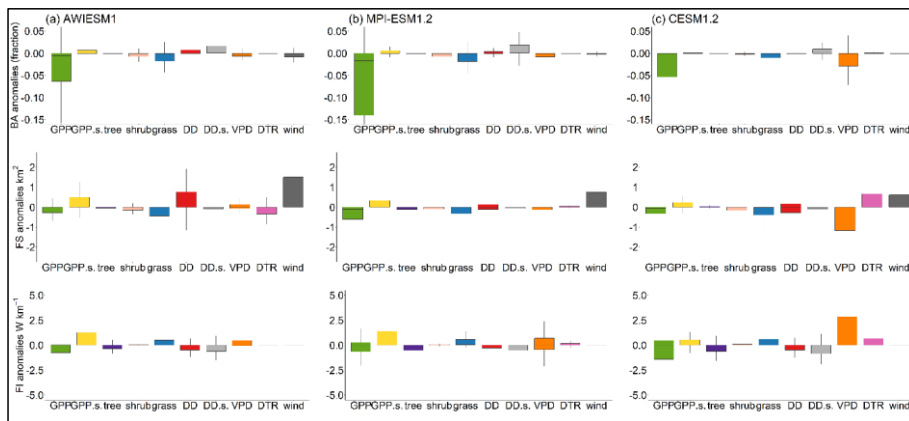
244

245 **Figure 3.** Experiments for BA, FS and FI for MPI-ESM1.2 LGM scenario (MOD 395 ppm and LGM 185 ppm
 246 represent the realistic modern-day simulation and LGM simulation, whilst MOD 185 ppm and LGM 395 ppm
 247 represent the CO₂ and climate sensitivity experiments respectively. The ice is shown in grey). (The other
 248 experiments can be found in S3)

249
 250 Under low CO₂ levels with MOD climate (MOD climate/LGM CO₂) global BA decreased by ~ 70%
 251 under all three LGM scenarios (72% for CESM1.2 and AWIESM1, 73% for MPI-ESM1.2). Despite larger global
 252 decreased BA compared to the realistic LGM scenarios, the number of grid cells in which no burning occurred
 253 was only 1.7 times higher for MPI-ESM1.2 and AWIESM1 LGM scenarios and 1.5 times CESM1.2 LGM
 254 scenario compared to the realistic MOD scenario. The spatial pattern was consistent across all three LGM
 255 scenarios, with very few grid-points showing a positive BA anomaly relative to the MOD experiment. Though FS
 256 increased slightly under this sensitivity experiment when burning did occur, this increase was concentrated in the
 257 tropical regions of South America and Africa (mainly Amazonia), (except for AWIESM1 were increases were
 258 observed across Eurasia). In burning grid-cells, global median FI increased by ~ 15-18% in this sensitivity
 259 experiment (18% for MPI-ESM1.2 and CESM1.2, and 15% for AWIESM1). This spatial pattern was also
 260 consistent as with BA, with very few negative FI anomalies, except for regions ~ 20-30°N and ~20-30°S.

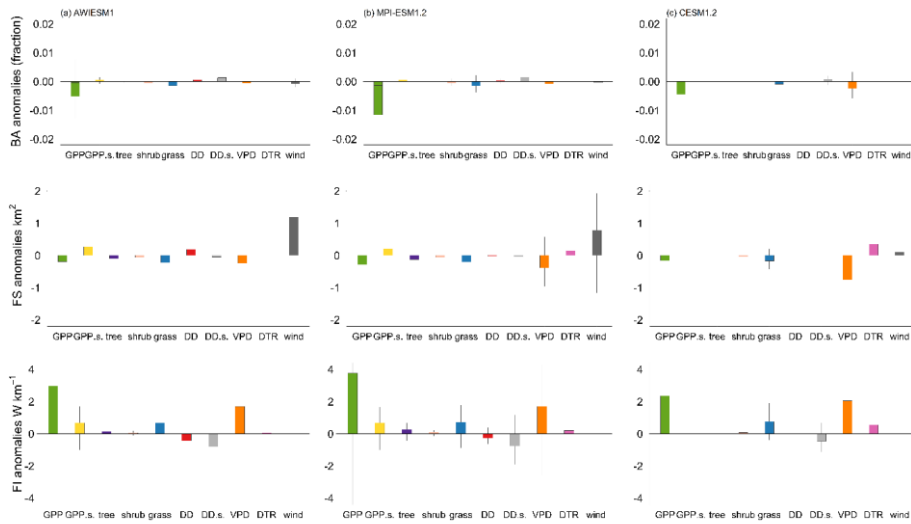
261 Under MOD CO₂ and LGM climate, BA decreased by 41% compared to the MOD experiment for the
 262 CESM1.2 LGM scenario and by 4% for the MPI-ESM1.2 LGM scenario but increased by 48% for the AWIESM1
 263 LGM scenario, showing a strong sensitivity to climate. The number of grid cells in which no burning occurred
 264 was of similar amplitude to the previous sensitivity experiment for the MPI-ESM1.2 and AWIESM1 LGM
 265 scenarios (~1.8 times higher compared to the realistic MOD scenario) but was much higher for the CESM1.2
 266 LGM scenario (~3.5 increase). When burning occurred, the global median FS increased under all LGM scenarios
 267 by 17% for CESM1.2, 25% for MPI-ESM1.2 and 23% for AWIESM1. These increases were concentrated in
 268 tropical Africa, central America, and Russia, with decreases shown in North America and South Africa. Global
 269 median FI also increased under this sensitivity experiment by 2-3% for AWIESM1 and MPI-ESM1.2 but
 270 decreased by 5% for CESM1.2 LGM scenario, with decreases concentrated in Eurasia and North America.

271



272

273



275

276

277

278

279

280

281

282

283

284

285

286

287

288

289

290

291

292

293

294

295

296

297

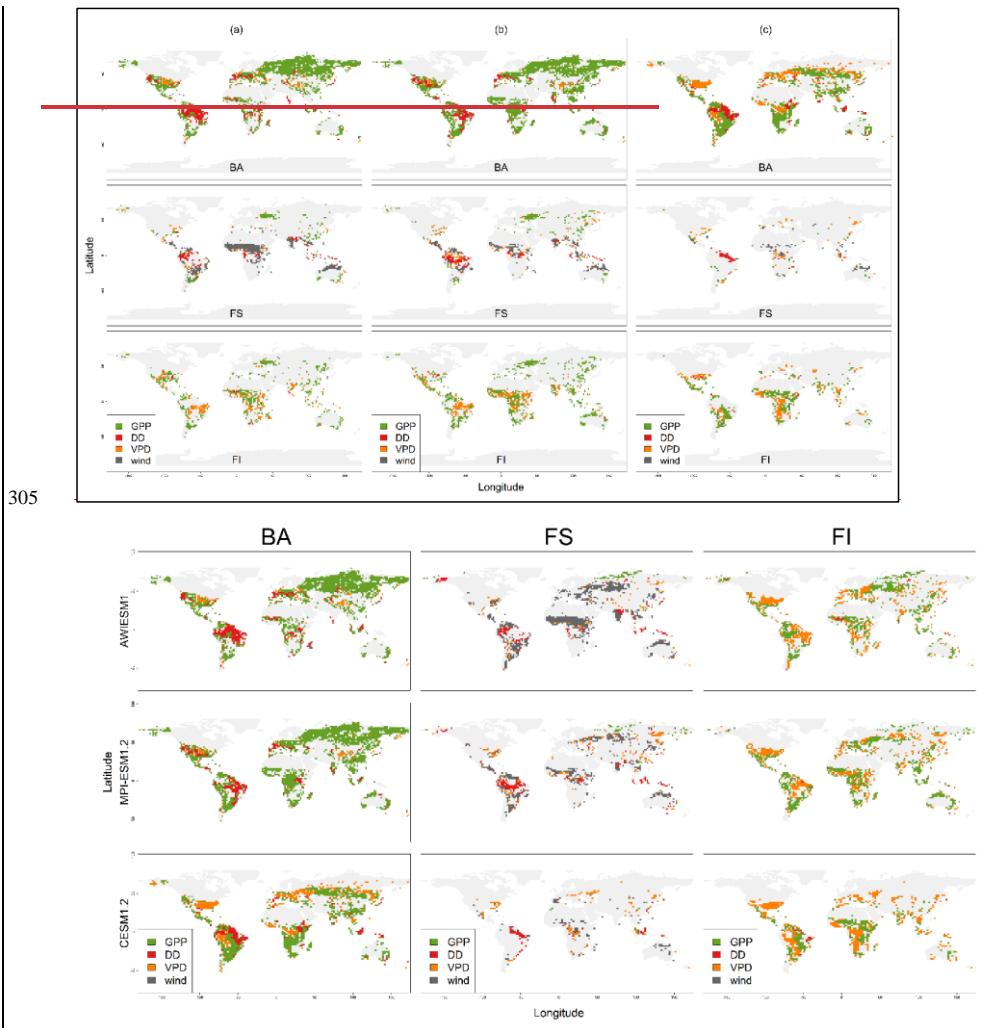
298

Figure 4. Boxplots showing relative importance of each predictor (GPP: gross primary production, GPP.s.: GPP seasonality, tree; tree cover, shrub; shrub cover, grass; grass cover, DD: dry days, DD.s.: dry days seasonality, VPD: vapour pressure deficit, DTR: diurnal temperature range, wind: wind speed) in driving the BA, FS or FI anomaly between the MOD 395 ppm and LGM 190 ppm experiment. For each grid cell common to both experiments (on modern-day continental shelves and masking the LGM ice sheets), the predictor which caused the largest change in the anomaly between the two experiments when it was excluded from the GLM model was retained, it is the change in anomaly that is shown here. This was taken as an indicator of relative importance of that predictor in driving the observed change for (a) the AWIESM1 LGM scenario, (b) the MPI-ESM1.2 LGM scenario and (c) the CESM1.2 LGM scenario. A positive anomaly indicates the variable caused an increase in BA, FS or FI at the LGM and a negative anomaly indicates the variable caused a decrease in BA, FS or FI at the LGM.

Reductions in BA between the MOD and LGM scenarios were driven primarily by changes in GPP, grass cover, VPD and to a lesser extent dryness (dry days (DD) and dry-day seasonality (DD.s)). Changes in FI were driven by changes in GPP as well as VPD, with changes in GPP seasonality also leading to increased FI in inland regions, reflecting both changes in climate and CO₂ levels for BA and FI. Increased FS was largely driven by increased wind speeds, as well as DD and diurnal temperature range (DTR) reflecting a strong climate effect as well as GPP seasonality. Decreases in FS driven were by changes in GPP and grass cover, as well as VPD under the CESM1.2 LGM scenario and DTR under the AWIESM1 LGM scenario (Figure 4). Changes in GPP and grass cover were responsible for the largest reductions in burning, with these vegetation effects concentrated across Africa and much of Eurasia (see Figure 5). In Amazonia, changes in DD were the most important factor, reducing BA and FS (except for MPI-ESM1.2 which saw increased FS driven by DD). Increased BA in western Alaska was driven by GPP in the MPI-ESM1.2 and AWIESM1 LGM scenarios. Increased BA in tropical regions were

Formatted: Indent: First line: 0 cm

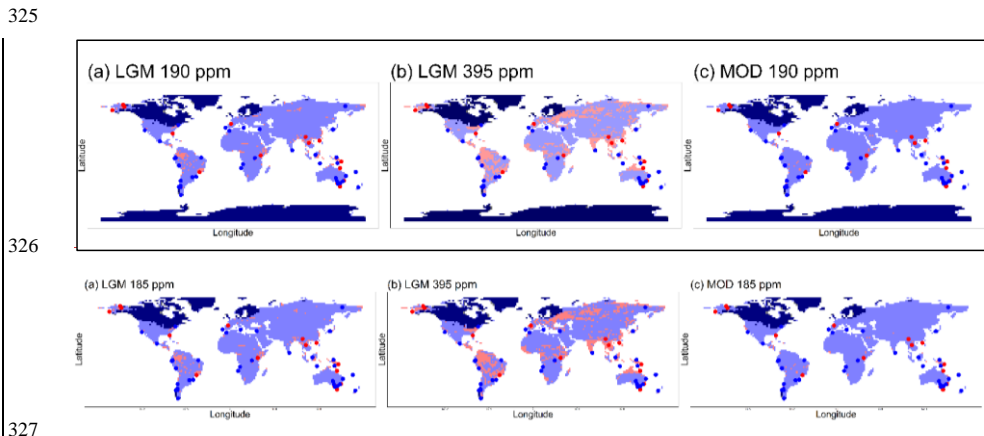
299 driven by grass cover, GPP and DD changes. Changes in VPD across the northern latitudes, especially of north
 300 America and Europe, led to decreased BA in the most conservative CESM1.2 LGM scenario. FS decreased across
 301 the Americas and Eurasia in the CESM1.2 LGM scenario because of low VPD values which reduced the
 302 occurrence of burning and offset the increases caused by wind speed and DTR in the other two LGM scenarios.
 303 Low values of VPD drove increases in FI across eastern North America, South America, western Africa, and
 304 South-East Asia.



306
 307
 308 **Figure 5.** Map showing selection of four variables (GPP in green, DD in red, VPD in orange and wind in grey)
 309 responsible for some of the most important grid-cell drivers in reducing BA, increasing FS and FI for (a)

310 AWIESM1 LGM scenario, (b) MPI-ESM1.2 LGM scenario and (c) CESM1.2 LGM scenario. Maps of most
 311 important grid-cell drivers for all variables and all experiments can be found in S3.

312
 313 Comparing the spatial patterns of the simulated BA anomalies with charcoal-based reconstructions of the sign of
 314 changes in biomass burning (RPD; Harrison et al., 2022) showed that the best overall match occurred when both
 315 the climate and CO₂ effect were considered, with a success rate of ~ 39-45% depending on the climate scenario.
 316 The MPI-ESM1.2 and AWIESM1 LGM scenarios produced the best overall matches. None of the MOD
 317 climate/LGM CO₂ experiments identified any of the positive BA anomalies shown by the charcoal records. The
 318 LGM climate/MOD CO₂ experiments identified around half (~ 10-17%) of the negative BA anomalies identified
 319 by the realistic experiment (17-20%) and the MOD climate/LGM CO₂ sensitivity experiment, and only performed
 320 marginally better than the realistic experiment in identifying the positive BA anomalies (Table 3). Thus, although
 321 this sensitivity experiment produced a similar overall agreement with the reconstructions as LGM climate/LGM
 322 CO₂ simulations, only the realistic scenarios produced similar success rates for both the negative and positive BA
 323 anomalies. ~~Climate change alone produced too few negative anomalies matches; CO₂ changes alone resulted in~~
 324 no positive anomaly matches.



326
 327
 328
 329 **Figure 6.** Comparison of BA anomalies between the BA experiment outputs from the MPI-ESM1.2 LGM
 330 scenario with charcoal records from the Reading Palaeofire Database (RPD) for (a) the realistic LGM
 331 experiment (b) the LGM climate/MOD CO₂ sensitivity experiment and (c) the MOD climate/LGM CO₂
 332 sensitivity experiment The modelled positive LGM-MOD anomalies are shown in red and LGM-MOD negative
 333 anomalies in blue. Dotted red (positive anomaly) and blue (negative anomaly) points show the location of the
 334 RPD records for the LGM. The LGM ice sheets are shown in dark blue.

335

BA experiments		MPI_ESM1.2			AWIESM1			CESM1.2 LGM		
Scenario	RPD	LGM	MOD	LGM	LGM	MOD	LGM	LGM	MOD	LGM
		190	190	395	190	190	395	190	190	395
Negative RPD anomalies										

Number of records	35	20	21	13	17	21	10	20	20	17
Successful identification (percentage)		57	60	37	49	60	29	57	57	49
Positive RPD anomalies										
Number of records	16	3	0	8	6	0	5	0	0	3
Successful identification (percentage)		19	0	50	38	0	31	0	0	19
Total RPD anomalies										
Number of records	51	23	21	21	23	21	15	20	20	20
Successful identification (percentage)		45	41	41	45	41	29	39	39	39

336

337 **Table 23.** Comparison of sign in BA anomalies (between the MOD climate/MOD CO₂ experiment and other
338 three experiments respectively) at the location of each RDP charcoal-based reconstruction record. A positive
339 anomaly represents increased biomass burning, and a negative anomaly represents decreased biomass burning.

340 A successful identification means that the sign of the experiment anomaly and the sign of the RDP charcoal-
341 based reconstructions are the same.

342

343 The sign of the charcoal records could reflect changes in FS or FI as well as BA. However, the success rates in
344 predicting the sign of the charcoal anomalies (both positive and negative) were not as good somewhat worse for
345 FS (27-31%) and FI (24-30%) than those obtained for BA for the realistic LGM experiment. Furthermore, both
346 FS and FI did not perform any better than BA under any experiment, with the sensitivity experiments matching
347 the charcoal anomalies slightly better for FS and FI than the realistic LGM experiment (see S4).

348 4. Discussion

349 Our simulations show a global reduction in burning at the LGM but increased median fire size and
350 intensity when burning did occur. BA, FS and FI were all sensitive to changes in vegetation driven directly by
351 CO₂ levels alone. BA and FI were most sensitive to this effect, with the climate effect dampening the effect of
352 CO₂ alone when both are included. The largest reductions in burning occurred when only the CO₂ effect was
353 considered although this experiment had fewer regions in which burning was excluded completely. This suggests
354 that the reduction in burning was more spatially consistent and widespread under these conditions than when both
355 effects were accounted for. The sensitivity of BA to CO₂ is explained by the reduction in fuel availability under
356 low CO₂, a strong constraint on burnt area. For FI, including a CO₂ effect also amplified the overall global signal.
357 This CO₂ effect is most likely driven by the negative relationship between GPP and FI fitted by the empirical
358 model. Whilst this relationship might seem counter-intuitive, it has a sound basis. The most intense fires occur in
359 regions with a seasonal variation in productivity rather than the most productive environments such as tropical
360 forests (Archibald et al., 2013). High productivity can (under some climate conditions) increase the frequency of
361 burning, which also reduces fuel loads (Rodrigues et al., 2019). Under appropriate climate conditions, there can
362 be long-term fuel build-up in areas of low productivity that is not offset by frequent burning. All these factors
363 help to explain why FI is not reduced at the LGM when burning occurs even though BA is. Low CO₂ decreased

364 FS except for tropical regions and reduced the impact of climate in the realistic scenarios. We hypothesize this is
365 because of decreased productivity leading to patchier vegetation, and hence reduced fuel continuity, which is a
366 factor limiting wildfire spread (Dial et al., 2022; Schertzer et al., 2015).

367 Changes in climate alone also affected all three modelled wildfire properties. The climate effect was
368 larger than the CO₂ effect across all models for FS, with increases in wind, DD and DTR driving the change. BA
369 was particularly sensitive to the amplitude of climate change: climate change alone greatly reduced BA under the
370 coldest LGM scenario (CESM1.2), had a limited effect in the intermediate LGM scenario (MPI-ESM1.2) and
371 increased BA in the warmest LGM scenario (AWIESM1). The amplitude of change in VPD, a measure of
372 atmospheric moisture, relative to other climate variables was especially important in influencing overall trends.
373 In the case of BA, large decreases in VPD under the CESM1.2 climate scenario led to much more substantial
374 reductions, most likely due to an increase in fuel moisture. Additionally, though stronger winds and increased
375 DTR were the main drivers of larger wildfires at the LGM, low VPD values in CESM1.2 severely limited FS and
376 FI in the northern latitudes. VPD has been shown to influence wildfire ignition and wildfire spread (Sedano &
377 Randerson, 2014), and our results suggest high atmospheric moisture can inhibit fire spread. When vegetation
378 was sufficiently abundant however, low VPD values were key in driving intensity. Although vegetation
379 productivity was lower at the LGM, decreased VPD may have contributed to larger fuel build-ups, thus increasing
380 fuel loads. This highlights the sensitivity of the fire regime not just to overall climate change but the relative
381 amplitude of change in individual climate variables.

382 Our model results reproduce the global reduction of biomass burning at the LGM observed from ice
383 cores and sedimentary charcoal records (Daniau et al., 2012; Harrison et al., 2022; Power et al., 2008; Rubino et
384 al., 2016). Some studies have indicated the occurrence of high-intensity wildfires on the Palaeo-Agulhas Plain of
385 South Africa, tropical regions, northern Australia, and central China at the LGM (Kraaij et al., 2020; Power et al.,
386 2008; Rowe et al., 2021; Ruan et al., 2020; M. Song et al., 2023). Our results are consistent with the trends in
387 these regions. The LGM simulations of BA that account for both climate and CO₂ appear to fit the charcoal records
388 best. The spatial patterns of BA at the LGM were more consistent with the patterns shown by sedimentary charcoal
389 records than FS and FI, consistent with the assumption that charcoal abundance can be used as a measure of
390 biomass burning. The FS and FI anomaly patterns ~~for both FS and FI~~ were less consistent than that of BA,
391 suggesting a regime of less burning but larger and more intense wildfires at the LGM could be consistent with the
392 charcoal records. Whilst FI has been reconstructed from charcoal (e.g. Duffin, 2008; Snitker, 2018) there are
393 currently no comparable measures that record FS or FI changes globally. Charcoal records are not available from
394 some regions, further limiting our ability to evaluate the models, particularly in Eurasia and inland South America
395 where low CO₂ leads to large reductions in BA that are not observed when only climate is considered. ~~The effect
396 of human activity was not considered in this analysis. Pre-agricultural hunter-gatherer populations used fire for
397 land management, for example to facilitate hunting and to promote the local abundance of food plants (Bowman,
398 1998; Gott, 2005), although recent work indicates that the burning regimes, they practiced tended to reduce fire
399 overall compared to the natural state (see e.g. Constantine IV et al., 2023). However, the areas suitable for hunter-
400 gatherer populations was much reduced at the LGM by generally colder and drier climates. It has been estimated
401 that less than 23% of Sahulland (the extended continent of Australia) and less than 58% of Africa was habitable at
402 the LGM (Gautney and Holliday, 2015; note Blinkhorn et al., 2022 estimate the range of habitable area as between
403 27 and 66%) and that hunter-gatherer populations were confined to climatically suitable refugia (see e.g. Williams~~

404 et al., 2013; Blinkhorn et al., 2022). Furthermore, although the estimates of population density are highly
405 uncertain, the LGM population of Australia was less than 5% of the modern population and the reduction in Africa
406 was even larger (Gautney and Holliday, 2015). Palaeoecological evidence from Australia suggests that the use of
407 fire by pre-agricultural hunter-gatherers had a low impact on the environment before the late Holocene (e.g. Black
408 et al., 2007; Fuller et al., 2014; Portenga et al., 2016). Thus, it is unlikely that human activities during the LGM
409 would have substantially increased fire or offset the impact of the changes in climate and CO₂ on fire regimes.

410 Our results are based on simple empirical models for BA, FS and FI. However, the inferred changes in
411 BA are similar to those of Martin Calvo et al. (2015) who used the Land surface Processes and eXchanges (LPX)
412 dynamic global vegetation model. Empirical models have been shown to perform as well as more complex
413 process-based models in simulating burned area under modern-day conditions (Hantson et al., 2020). Thus, our
414 conclusions about the relative impact of climate and CO₂ changes on fire properties are unlikely to be adversely
415 affected by the relative simplicity of the models used. Their simplicity facilitates running multiple scenarios and
416 diagnosis of the factors influencing changes in wildfire properties.

417 The effect of human activity was not considered in this analysis and as such no conclusions can be drawn
418 on how human activity may affect these trends. Although this is a limitation, we believe it is unlikely that human
419 activity would substantially impact the response of wildfire regimes to the changes in climate and CO₂ observed
420 here. Pre-agricultural hunter-gatherer populations used fire for land management, for example to facilitate hunting
421 and to promote the local abundance of food plants (Bowman, 1998; Gott, 2005), although recent work indicates
422 that the burning regimes they practiced tended to reduce fire overall compared to the natural state (see e.g.
423 Constantine IV et al., 2023). However, the areas suitable for hunter-gatherer populations was much reduced at the
424 LGM by generally colder and drier climates and hunter-gatherer populations were confined to climatically suitable
425 refugia (see e.g. Williams et al., 2013; Blinkhorn et al., 2022). Furthermore, although the estimates of population
426 density are highly uncertain, the LGM population of Australia was less than 5% of the modern population and the
427 reduction in Africa was even larger (Gautney and Holliday, 2015). Palaeoecological evidence from Australia
428 suggests that the use of fire by pre-agricultural hunter-gatherers had a low impact on the environment before the
429 late Holocene (e.g. Black et al., 2007; Fuller et al., 2014; Portenga et al., 2016). Thus, it is unlikely that human
430 activities during the LGM would have substantially increased fire or offset the impact of the changes in climate
431 and CO₂ on fire regimes. Previous studies show a weak influence of population and land-use change on driving
432 global wildfire trends prior to the 18th century (e.g. Pechony and Shindell, 2010; Bowman et al., 2020) and a sharp
433 human-driven decline in wildfire activity since the mid-nineteenth century (e.g. Marlon et al., 2008; Wang et al.,
434 2010). This recent reduction in global biomass burning was most likely driven by population growth and land-use
435 change leading to increased landscape fragmentation, which tends to suppress fire spread (e.g. Knorr et al., 2014;
436 Andela et al., 2016; Harrison et al., 2021).

437 These results add to a growing body of literature highlighting the importance of considering not only
438 changes in wildfire weather but also vegetation properties in projections of future wildfire regimes (e.g. Harrison
439 et al., 2021; Kuhn-Régnier et al., 2021; Pausas & Keeley, 2021). The impact of rising CO₂ levels will most likely
440 enhance vegetation growth and litter accumulation, which are important controls on fuel availability, continuity,
441 and load. However, climate and specifically VPD may have opposing effects to that of rising CO₂ levels. Since
442 VPD controls plant growth, increasing VPD can limit ecosystem productivity and tree growth, in turn reducing
443 fuel loads (Williams et al. 2013). Nevertheless, VPD has also been shown to increase litter fall, thus increasing

444 available dead fuel (Resco de Dios 2020, De Faria et al. 2017). As such, it is important to consider how temporal
445 and spatial scales affect the response of vegetation to changing VPD (Grossiord et al., 2020). Although the trade-
446 offs between future increases in CO₂ and reductions in productivity due to higher temperatures and atmospheric
447 dryness are not fully understood, this work highlights the importance of considering both. These effects will most
448 likely not be evenly distributed across the globe (Gonsamo et al., 2021; Piao et al., 2020; van der Sleen et al.,
449 2015) and CO₂ effects may be more important in some regions than others. In fuel-limited ecosystems, CO₂
450 fertilization could increase fuel loads and fuel continuity, increasing overall burnt area but also the potential for
451 larger and more intense wildfires. This is particularly worrying in regions with anticipated decreases in
452 atmospheric moisture, especially since evidence suggests rising VPD may only counteract a small proportion of
453 CO₂-induced plant growth (Y. Song et al., 2022). Increased woody thickening, for example in tropical South Asia
454 (Kumar et al., 2021; Scheiter et al., 2020), may also alter fuel loads in regions that are likely to be vulnerable to
455 ignition under a drier and warmer atmosphere (Clarke et al., 2022). Whilst climate variables such as DD and DTR
456 have also shown to be strong controls of global wildfires regimes (e.g. Bistinas et al., 2014; Forkel et al., 2019;
457 Kuhn-Régnier et al., 2021), this study highlights the importance of VPD relative to other climate variables in
458 driving spatial patterns of BA, FS and FI. This is in line with previous studies that have highlighted the important
459 role of VPD in promoting fuel loads and fire spread (e.g. Diffenbaugh et al., 2021; Grillakis et al., 2022; Duane
460 et al., 2021; Balch et al., 2022). These results add to a growing body of literature highlighting the importance of
461 considering not only changes in wildfire weather but also vegetation properties in projections of future wildfire
462 regimes (e.g. Harrison et al., 2021; Kuhn-Régnier et al., 2021; Pausas & Keeley, 2021). The impact of rising CO₂
463 levels will most likely enhance vegetation growth and litter accumulation, which are important controls on fuel
464 availability, continuity, and load. Although the trade-offs between future increases in CO₂ and reductions in
465 productivity due to higher temperatures and atmospheric dryness are not fully understood, this work highlights
466 the importance of considering both. These effects will most likely not be evenly distributed across the globe
467 (Gonsamo et al., 2021; Piao et al., 2020; van der Sleen et al., 2015) and CO₂ effects may be more important in
468 some regions than others. In fuel limited ecosystems, CO₂ fertilization could increase fuel loads and fuel
469 continuity, increasing overall burnt area but also the potential for larger and more intense wildfires. This is
470 particularly worrying in regions with anticipated decreases in atmospheric moisture, especially since evidence
471 suggests rising VPD may only counteract a small proportion of CO₂-induced plant growth (Y. Song et al., 2022).
472 Increased woody thickening, for example in tropical South Asia (Kumar et al., 2021; Scheiter et al., 2020), may
473 also alter fuel loads in regions that are likely to be vulnerable to ignition under a drier and warmer atmosphere
474 (Clarke et al., 2022). This work also highlights the role of VPD in promoting fuel loads and limiting fire ignition
475 and fire spread, a climatic variable that has been linked wildfire occurrence (Diffenbaugh et al., 2021). Although
476 the effect of human activity was not considered in this analysis, if reductions in burnt area do contribute to greater
477 fuel loads, suppression policies may artificially increase fuel loads in the same way reduced burnt area increased
478 fuel loads under LGM conditions, suggesting resulting wildfires may be larger and more intense. Correctly
479 projecting changes in fuels in the next century will require considering both the effect of VPD and effects of CO₂
480 on plant growth and fuel loads.

481 Our results stress the importance of accounting for the effects of CO₂ on vegetation when considering
482 how future fire regimes may evolve. Different aspects of the fire regime respond differently to changes in fuel
483 properties. Without accounting for this crucial effect, our understanding of future risks will remain limited.

484
485
486
487
488
489
490
491
492
493
494
495
496
497
498
499
500
501
502
503
504
505
506
507
508
509
510
511

512
513
514
515
516
517
518
519
520
521
522

Code availability. All code used in this paper is available at freely available for use in RStudio: the code for the GLM models is available at <https://doi.org/10.6084/m9.figshare.19071044.v1>, and the code to generate the experiments are available at: <https://doi.org/10.6084/m9.figshare.22285303.v2> and <https://doi.org/10.6084/m9.figshare.22285279.v2>.

Data availability: All LGM data can be retrieved from <https://esgf-node.llnl.gov/projects/cmip6/>, all modern data can be retrieved from references provided. The P Model documentation is available at <https://pyrealm.readthedocs.io/en/latest/> and the BIOME4 documentation is available at <https://pmip2.lsce.ipsl.fr/synth/biome4.shtml> and <https://github.com/jedokaplan/BIOME4>.

Author contributions. Experiments conception, strategy and interpretation were developed by O H, ICP and SPH jointly. OH performed the data processing and analysis, and produced the graphics and Tables. OH wrote the original draft; SPH and ICP contributed to the final draft.

Competing interests. The contact author has declared that neither themselves nor any other authors have a conflict of interest.

Acknowledgements and financial support. OH acknowledges support from the NERC Centre for Doctoral Training in Quantitative and Modelling skills in Ecology and Evolution (Grant No. NE/S007415/1) and from the Leverhulme Trust through the Leverhulme Centre for Wildfires, Environment and Society (Grant No. RC-2018-023). Special thanks to David Orme for this help with setting up BIOME4. ICP acknowledges support from the European Research Council (787203 REALM) under the European Union’s Horizon 2020 research programme. SPH is supported by the European Research Council (694481 GC2.0) under the same programme. This work is a contribution to the LEMONTREE (Land Ecosystem Models based On New Theory, obseRvations and ExperimEnts) project, funded through the generosity of Eric and Wendy Schmidt by recommendation of the Schmidt Futures program.

References

Abatzoglou, J. T., Williams, A. P., & Barbero, R. (2019). Global emergence of anthropogenic climate change in fire weather indices. *Geophysical Research Letters*, *46*(1), 326–336.

Albani, S., Balkanski, Y., Mahowald, N., Winckler, G., Maggi, V., & Delmonte, B. (2018). Aerosol-climate interactions during the Last Glacial Maximum. In *Current Climate Change Reports* (Vol. 4, Issue 2, pp. 99–114). Springer. <https://doi.org/10.1007/s40641-018-0100-7>

Andela, N., Morton, D. C., Giglio, L., Paugam, R., Chen, Y., Hantson, S., Van Der Werf, G. R., & Randerson, J. T. (2019). The Global Fire Atlas of individual fire size, duration, speed and direction. *Earth System Science Data*, *11*(2), 529–552.

Archibald, S., Lehmann, C. E. R., Gómez-Dans, J. L., & Bradstock, R. A. (2013). Defining pyromes and global syndromes of fire regimes. *Proceedings of the National Academy of Sciences*, *110*(16), 6442–6447.

523 Balch, J.K., Abatzoglou, J.T., Joseph, M.B., Koontz, M.J., Mahood, A.L., McGlinchy, J., Cattau, M.E. and
524 Williams, A.P., 2022. Warming weakens the night-time barrier to global fire. *Nature*, 602(7897), pp.442-
525 448.

526 Bistinas, I., Harrison, S.P., Prentice, I.C. and Pereira, J.M.C., 2014. Causal relationships versus
527 emergent patterns in the global controls of fire frequency. *Biogeosciences*, 11(18), pp.5087-5101.
528

529 Betts, R. A., Golding, N., Gonzalez, P., Gornall, J., Kahana, R., Kay, G., Mitchell, L., & Wiltshire, A. (2015).
530 Climate and land use change impacts on global terrestrial ecosystems and river flows in the HadGEM2-ES
531 Earth system model using the representative concentration pathways. *Biogeosciences*, 12(5), 1317–1338.

532 Black, M. P., Mooney, S. D., & Haberle, S. G. (2007). The fire, human and climate nexus in the Sydney Basin,
533 eastern Australia. *The Holocene*, 17(4), 469-480.

534 Blinkhorn, J., Timbrell, L., Grove, M., & Scerri, E. M. L. (2022). Evaluating refugia in recent human evolution
535 in Africa. *Philosophical Transactions of the Royal Society B*, 377(1849), 20200485.

536 Bond, W. J., & Midgley, G. F. (2012). Carbon dioxide and the uneasy interactions of trees and savannah grasses.
537 *Philosophical Transactions of the Royal Society B: Biological Sciences*, 367(1588), 601–612.

538 Bond, W. J., Midgley, G. F., & Woodward, F. I. (2003). The importance of low atmospheric CO₂ and fire in
539 promoting the spread of grasslands and savannas. *Global Change Biology*, 9(7), 973–982.

540 Bowman, D. M. J. S. (1998). The impact of Aboriginal landscape burning on the Australian biota. *The New*
541 *Phytologist*, 140(3), 385–410.

542 Bowman, D. M. J. S., Kolden, C. A., Abatzoglou, J. T., Johnston, F. H., van der Werf, G. R., & Flannigan, M.
543 (2020). Vegetation fires in the Anthropocene. *Nature Reviews Earth & Environment*, 1(10), 500–515.

544 Bradstock, R. A. (2010). A biogeographic model of fire regimes in Australia: current and future implications.
545 *Global Ecology and Biogeography*, 19(2), 145–158.

546 Bragg, F. J., Prentice, I. C., Harrison, S. P., Eglinton, G., Foster, P. N., Rommerskirchen, F., & Rullkötter, J.
547 (2013). Stable isotope and modelling evidence for CO₂ as a driver of glacial–interglacial vegetation shifts
548 in southern Africa. *Biogeosciences*, 10(3), 2001–2010.

549 Buitenwerf, R., Bond, W. J., Stevens, N., & Trollope, W. (2012). Increased tree densities in South African
550 savannas: > 50 years of data suggests CO₂ as a driver. *Global Change Biology*, 18(2), 675–684.

551 Clarke, H., Nolan, R. H., de Dios, V. R., Bradstock, R., Griebel, A., Khanal, S., & Boer, M. M. (2022). Forest fire
552 threatens global carbon sinks and population centres under rising atmospheric water demand. *Nature*
553 *Communications*, 13(1), 7161. <https://doi.org/10.1038/s41467-022-34966-3>

554 Constantine IV, M., Williams, A. N., Francke, A., Cadd, H., Forbes, M., Cohen, T. J., Zhu, X., & Mooney, S. D.
555 (2023). Exploration of the burning question: a long history of fire in eastern Australia with and without
556 people. *Fire*, 6(4), 152.

557 Cucchi, M., Weedon, G. P., Amici, A., Bellouin, N., Lange, S., Müller Schmied, H., Hersbach, H., & Buontempo,
558 C. (2020). WFDE5: bias-adjusted ERA5 reanalysis data for impact studies. *Earth System Science Data*,
559 12(3), 2097–2120.

560 Daniaux, A.-L., Bartlein, P.J., Harrison, S.P., Prentice, I.C., Brewer, S., Friedlingstein, P., Harrison-Prentice, T.I.,
561 Inoue, J., Marlon, J.R., Mooney, S., Power, M.J., Stevenson, J., Tinner, W., Andrić, M., Atanassova, J.,
562 Behling, H., Black, M., Blarquez, O., Brown, K. J., Carcaillet, C., Colhoun, E., Colombaroli, D., Davis,

Formatted: Font: Italic

Formatted: Normal, Left, Indent: Hanging: 0.85 cm, Line spacing: single, Don't adjust space between Latin and Asian text, Don't adjust space between Asian text and numbers

Formatted: Font: 10 pt, Font color: Auto, Pattern: Clear

Formatted: Indent: First line: 0 cm

Formatted: Indent: Left: 0 cm

Formatted: Font: Italic

Formatted: Font: Italic

Formatted: Font: Italic

Formatted: Font: Italic

- 563 B.A.S., D’Costa, D., Dodson, J., Dupont, L., Eshetu, Z., Gavin, D.G., Genries, A., Gebru, T., Haberle, S.,
 564 Hallett, D. J., Horn, S., Hope, G., Katamura, F., Kennedy, L., Kershaw, P., Krivonogov, S., Long, C., Magri,
 565 D., Marinova, E., McKenzie, G.M., Moreno, P.I., Moss, P., Neumann, F.H., Norström, E., Paitre, C., Rius,
 566 D., Roberts, N., Robinson, G., Sasaki, N., Scott, L., Takahara, H., Terwilliger, V., Thevenon, F., Turner,
 567 R.B., Valsecchi, V.G., Vannière, B., Walsh, M., Williams, N., & Zhang, Y. (2012). Predictability of biomass
 568 burning in response to climate changes. *Global Biogeochemical Cycles* 26: GB4007,
 569 doi:10.1029/2011GB004249.
- 570 De Dios, V.R., Hedou, J., Camprubí, À.C., Thapa, P., Del Castillo, E.M., de Aragón, J.M., Bonet, J.A., Balaguer-
 571 Romano, R., Díaz-Sierra, R., Yebra, M. and Boer, M.M., 2021. Climate change induced declines in fuel
 572 moisture may turn currently fire-free Pyrenean mountain forests into fire-prone ecosystems. *Science of The*
 573 *Total Environment*, 797, p.149104.
- 574 De Faria, B.L., Brando, P.M., Macedo, M.N., Panday, P.K., Soares-Filho, B.S. and Coe, M.T., 2017. Current and
 575 future patterns of fire-induced forest degradation in Amazonia. *Environmental Research Letters*, 12(9),
 576 p.095005.
- 577 Dial, R. J., Maher, C. T., Hewitt, R. E., & Sullivan, P. F. (2022). Sufficient conditions for rapid range expansion
 578 of a boreal conifer. *Nature*, 608(7923), 546–551. <https://doi.org/10.1038/s41586-022-05093-2>
- 579 Diffenbaugh, N. S., Konings, A. G., & Field, C. B. (2021). Atmospheric variability contributes to increasing
 580 wildfire weather but not as much as global warming. *Proceedings of the National Academy of Sciences*,
 581 118(46), e2117876118. <https://doi.org/10.1073/pnas.2117876118>
- 582 Donohue, R. J., Roderick, M. L., McVicar, T. R., & Farquhar, G. D. (2013). Impact of CO₂ fertilization on
 583 maximum foliage cover across the globe’s warm, arid environments. *Geophys. Res. Lett.*, 40, 3031–3035.
 584 <https://doi.org/10.1002/grl.50563>.
- 585 Duane, A., Castellnou, M. and Brotons, L., 2021. Towards a comprehensive look at global drivers of novel
 586 extreme wildfire events. *Climatic Change*, 165(3-4), p.43
- 587 Duffin, K. I. (2008). The representation of rainfall and fire intensity in fossil pollen and charcoal records from a
 588 South African savanna. *Review of Palaeobotany and Palynology*, 151(1–2), 59–71.
- 589 Flannigan, M., Cantin, A. S., De Groot, W. J., Wotton, M., Newbery, A., & Gowman, L. M. (2013). Global
 590 wildland fire season severity in the 21st century. *Forest Ecology and Management*, 294, 54–61.
- 591 Fuller, D. Q., Denham, T., Arroyo-Kalin, M., Lucas, L., Stevens, C. J., Qin, L., Allaby, R. G., & Purugganan, M.
 592 D. (2014). Convergent evolution and parallelism in plant domestication revealed by an expanding
 593 archaeological record. *Proceedings of the National Academy of Sciences*, 111(17), 6147–6152.
- 594 Gautney, J. R., & Holliday, T. W. (2015). New estimations of habitable land area and human population size at
 595 the Last Glacial Maximum. *Journal of Archaeological Science*, 58, 103–112.
- 596 Gonsamo, A., Ciais, P., Miralles, D. G., Sitch, S., Dorigo, W., Lombardozzi, D., Friedlingstein, P., Nabel, J. E.
 597 M. S., Goll, D. S., & O’Sullivan, M. Arneith, A., Anthoni, P., Jain, A.K., Wiltshire A., Peylin P., Cescatti
 598 A. (2021). Greening drylands despite warming consistent with carbon dioxide fertilization effect. *Global*
 599 *Change Biology*, 27(14), 3336–3349.
- 600 Gott, B. (2005). Aboriginal fire management in south-eastern Australia: aims and frequency. *Journal of*
 601 *Biogeography*, 1203–1208.

Formatted: Font: Italic

Formatted: Font: Italic

Formatted: Font: Italic

Formatted: Font: Italic

Formatted: Font: Italic

602 Grillakis, M., Voulgarakis, A., Rovithakis, A., Seiradakis, K.D., Koutroulis, A., Field, R.D., Kasoar, M.,
603 Papadopoulos, A. and Lazaridis, M., 2022. Climate drivers of global wildfire burned area. *Environmental*
604 *Research Letters*, 17(4), p.045021.

Formatted: Font: Italic

605 Grossiord, C., Buckley, T.N., Cernusak, L.A., Novick, K.A., Poulter, B., Siegwolf, R.T., Sperry, J.S. and
606 McDowell, N.G., 2020. Plant responses to rising vapor pressure deficit. *New Phytologist*, 226(6), pp.1550-
607 1566.

Formatted: Font: Italic

608 Haas, O., Prentice, I. C., & Harrison, S. P. (2022). Global environmental controls on wildfire burnt area, size, and
609 intensity. *Environmental Research Letters*, 17(6), 065004.

610 Haas, Olivia (2023): Scripts and input files. figshare. Dataset. <https://doi.org/10.6084/m9.figshare.19071044.v1>

611 Haas, Olivia (2023): Data for: The response of wildfire regimes to Last Glacial Maximum carbon dioxide and
612 climate. figshare. Dataset. <https://doi.org/10.6084/m9.figshare.22285303.v2>

613 Haas, Olivia (2023): R scripts to run models for: The response of wildfire regimes to Last Glacial Maximum
614 carbon dioxide and climate. figshare. Software. <https://doi.org/10.6084/m9.figshare.22285279.v2>

615 Hantson, S., Kelley, D. I., Arneth, A., Harrison, S. P., Archibald, S., Bachelet, D., Forrest, M., Hickler, T., Lasslop,
616 G., Li, F., Mangeon, S., Melton, J.R., Nieradzki, L., Rabin, S.S., Prentice, I.C., Sheehan, T., Sitch, S.,
617 Teckentrup, L., Voulgarakis, A., & Yue, C. (2020). Quantitative assessment of fire and vegetation
618 properties in simulations with fire-enabled vegetation models from the Fire Model Intercomparison Project.
619 *Geoscientific Model Development*, 13(7), 3299–3318.

620 Harrison, S. P., & Prentice, C. I. (2003). Climate and CO₂ controls on global vegetation distribution at the last
621 glacial maximum: analysis based on palaeovegetation data, biome modelling and palaeoclimate simulations.
622 *Global Change Biology*, 9(7), 983–1004.

623 Harrison, S. P., Prentice, I. C., Bloomfield, K. J., Dong, N., Forkel, M., Forrest, M., Ningthoujam, R. K.,
624 Pellegrini, A., Shen, Y., & Baudena, M. Cardoso, A.W., Huss, J.C., Joshi J., Oliveras, I., Pausas, J.G. and
625 Simpson, J.K. (2021). Understanding and modelling wildfire regimes: an ecological perspective.
626 *Environmental Research Letters*, 16(12), 125008.

627 Harrison, S.P., Villegas-Diaz, R., Cruz-Silva, E., Gallagher, D., Kesner, D., Lincoln, P., Shen, Y., Sweeney, L.,
628 Colombaroli, D., Ali, A., Barhoumi, C., Bergeron, Y., Blyakharchuk, T., Bobek, P., Bradshaw, R., Clear,
629 J.L., Czerwiński, S., Daniau, A-L., Dodson, J., Edwards, K.J., Edwards, M.E., Feurdean, A., Foster, D.,
630 Gajewski, K., Gałka, M., Gameau, M., Giesecke, T., Gil Romera, G., Girardin, M.P., Hofer, D., Huang,
631 K., Inoue, J., Jamrichová, E., Jasiunas, N., Jiang, W., Jiménez-Moreno, G., Karpińska-Kołaczek, M.,
632 Kołaczek, P., Kuosmanen, N., Lamentowicz, M., Lavoie, M., Li, F., Li, J., Lisitsyna, O., López-Sález, J.A.,
633 Luelmo-Lautenschlaeger, R., Magnan, G., Magyari, E.K., Maksims, A., Marcisz, K., Marinova, E., Marlon,
634 J., Mensing, S., Mirosław-Grabowska, J., Oswald, W., Pérez-Díaz, S., Pérez-Obiol, R., Piilo, S., Poska, A.,
635 Qin, X., Remy, C.C., Richard, P.J.H., Salonen, S., Sasaki, N., Schneider, H., Shoty, W., Stancikaite, M.,
636 Štejnberga, D., Stivrins, N., Takahara, H., Tan, Z., Trasune, L., Umbanhowar, C.E., Văliranta, M., Vassiljev,
637 J., Xiao, X., Xu, Q., Xu, X., Zawisza, E., Zhao, Y., Zhou, Z., & Paillard, J. (2022). The Reading Palaeofire
638 database: an expanded global resource to document changes in fire regimes from sedimentary charcoal
639 records *Earth System Science Data* 14: 1109-1124 <https://doi.org/10.5194/essd-14-1109-2022>

640 Humber, M. L., Boschetti, L., Giglio, L., & Justice, C. O. (2019). Spatial and temporal intercomparison of four
641 global burned area products. *International Journal of Digital Earth*, 12(4), 460–484.

642 Jolly, W. M., Cochrane, M. A., Freeborn, P. H., Holden, Z. A., Brown, T. J., Williamson, G. J., & Bowman, D.
643 M. J. S. (2015). Climate-induced variations in global wildfire danger from 1979 to 2013. *Nature*
644 *Communications*, 6(1), 1–11.

645 Kageyama, M., Harrison S.P., Kapsch, M.L., Lofverstrom, M., Lora J.M., Mikolajewicz U., Sherriff-Tadano,S.,
646 Vadsaria T., Abe-Ouchi A., Bouttes N., Chandan, D., Gregoire L.J., Ivanovic, R.F., Kenji Izumi, Allegra
647 N. LeGrande, Fanny Lhardy, Gerrit Lohmann, Polina A. Morozova, Rumi Ohgaito, Paul, Peltier W.R.,
648 Poulsen, C.J., Quiquet, A., Roche, D.M., Shi, X., Tierney, J.E., Valdes, P.J., Volodin E. & Zhu J. (2021).
649 The PMIP4-CMIP6 Last Glacial Maximum experiments: preliminary results and comparison with the
650 PMIP3-CMIP5 simulations. *Climate of the Past* 17: 1065-1089

651 Kaplan, J.O., Bigelow, Prentice, I.C., Harrison, S.P., P.J., N.H., Bartlein, Christensen, T.R., Cramer, W.,
652 Matveyeva, N.V., McGuire, A.D., Murray, D.F., Razzhivin, V.Y., Smith, B. and Walker, D.A., Anderson,
653 P.M., Andreev, A.A., Brubaker, L.B., Edwards, M.E., & Lozhkin, A.V. (2003). Climate change and Arctic
654 ecosystems II: Modeling, palaeodata-model comparisons, and future projections. *Journal of Geophysical*
655 *Research-Atmosphere* 108, No. D19, 8171. (DOI: 10.1029/2002JD002559).

656 Kaplan, J. O., Pfeiffer, M., Kolen, J. C. A., & Davis, B. A. S. (2016). Large scale anthropogenic reduction of
657 forest cover in Last Glacial Maximum Europe. *PLoS One*, 11(11), e0166726.

658 Kgope, B. S., Bond, W. J., & Midgley, G. F. (2010). Growth responses of African savanna trees implicate
659 atmospheric [CO₂] as a driver of past and current changes in savanna tree cover. *Austral Ecology*, 35(4),
660 451–463.

661 Knorr, W., Jiang, L., & Arneith, A. (2016). Climate, CO₂ and human population impacts on global wildfire
662 emissions. *Biogeosciences*, 13(1), 267–282.

663 [Knorr, W., Kaminski, T., Arneith, A. and Weber, U., 2014. Impact of human population density on fire frequency](#)
664 [at the global scale. *Biogeosciences*, 11\(4\), pp.1085-1102.](#)

665 Kraaij, T., Engelbrecht, F., Franklin, J., & Cowling, R. M. (2020). A fiery past: A comparison of glacial and
666 contemporary fire regimes on the Palaeo-Agulhas Plain, Cape Floristic Region. *Quaternary Science*
667 *Reviews*, 235, 106059.

668 Kuhn-Régnier, A., Voulgarakis, A., Nowack, P., Forkel, M., Prentice, I. C., & Harrison, S. P. (2021). The
669 importance of antecedent vegetation and drought conditions as global drivers of burnt area. *Biogeosciences*,
670 18(12), 3861–3879.

671 Kumar, D., Pfeiffer, M., Gaillard, C., Langan, L., & Scheiter, S. (2021). Climate change and elevated CO₂ favor
672 forest over savanna under different future scenarios in South Asia. *Biogeosciences*, 18(9), 2957–2979.

673 Li, F., Levis, S., & Ward, D. S. (2013). Quantifying the role of fire in the Earth system - Part I: Improved global
674 fire modeling in the Community Earth System Model (CESM1). *Biogeosciences*, 10(4), 2293–2314.
675 <https://doi.org/10.5194/bg-10-2293-2013>

676 Li, W., MacBean, N., Ciais, P., Defourny, P., Lamarche, C., Bontemps, S., Houghton, R. A., & Peng, S. (2018).
677 Gross and net land cover changes in the main plant functional types derived from the annual ESA CCI land
678 cover maps (1992–2015). *Earth System Science Data*, 10(1), 219–234

679 [-Liu, L., Bestel, S., Shi, J., Song, Y., & Chen, X. \(2013\). Paleolithic human exploitation of plant foods during the](#)
680 [last glacial maximum in North China. *Proceedings of the National Academy of Sciences of the United States*](#)
681 [of America, 110\(14\), 5380–5385. <https://doi.org/10.1073/pnas.1217864110>](#)

Formatted: Indent: Hanging: 0.85 cm, Line spacing: 1.5 lines, Don't adjust space between Latin and Asian text, Don't adjust space between Asian text and

Formatted: Font color: Auto

682
683 Lohmann, G., Butzin, M., Eissner, N., Shi, X., & Stepanek, C. (2020). Abrupt climate and weather changes across
684 time scales. *Paleoceanography and Paleoclimatology*, 35(9), e2019PA003782.

685 Marlon, J.R., Bartlein, P.J., Carcaillet, C., Gavin, D.G., Harrison, S.P., Higuera, P.E., Joos, F., Power, M.J. and
686 Prentice, I.C., 2008. Climate and human influences on global biomass burning over the past two millennia.
687 *Nature Geoscience*, 1(10), pp.697-702.

688 Marlon, J. R., Kelly, R., Daniou, A.-L., Vanni re, B., Power, M. J., Bartlein, P., Higuera, P., Blarquez, O., Brewer,
689 S., Br ucher, T., Feurdean A., Romera G.G., Iglesias V., Maezumi S.Y., Magi, B., Courtney Mustaphi, C.J.,
690 & Zhihai, T. (2016). Reconstructions of biomass burning from sediment-charcoal records to improve data-
691 model comparisons. *Biogeosciences*, 13(11), 3225–3244.

692 Martin Calvo, M., & Prentice, I. C. (2015). Effects of fire and CO₂ on biogeography and primary production in
693 glacial and modern climates. *New Phytologist*, 208(3), 987–994.

694 Martin Calvo, M., Prentice, I. C., & Harrison, S. P. (2014). Climate versus carbon dioxide controls on biomass
695 burning: a model analysis of the glacial–interglacial contrast. *Biogeosciences*, 11(21), 6017–6027.

696 Mauritsen, T., Bader, J., Becker, T., Behrens, J., Bittner, M., Brokopf, R., Brovkin, V., Claussen, M., Crueger, T.,
697 Esch, M., Fast I., Fiedler S., Fl schner D., Gayler V., Giorgetta M., Goll D.S., Haak H., Hagemann S.,
698 Hedemann C., Hohenegger C., Ilyina, T., Jahns T., Jimen ez-de-la-Cuesta, D., Jungclaus J., Kleinen T.,
699 Kloster S., Kracher D., Kinne S., Kleberg D., Lasslop G., Kornblueh L., Marotzke J., Matei D., Meraner K.,
700 Mikolajewicz U., Modali K., M obis, B., M uller A.W., Julia E. M. S. Nabel, J.E. M. S. Nam C.C.W., Notz
701 D., Nyawira S., Paulsen H., Peters K., Pincus R., Pohlmann H., Pongratz J., Popp M., J rgen Raddatz T.,
702 Rast S., Redler,R., Reick, C.H., Rohrschneider, T., Schemann V., Schmidt, H., Schnur R., Schulzweida, U.,
703 Six K.D., Stein, L., Stemmler, I., Stevens B., Storch J-S.V, Tian F., Voigt, A., Vrese, P., Wieners K.,
704 Wilkenskjeld, S., Winkler A., Roeckner, E. (2019). Developments in the MPI-M Earth System Model
705 version 1.2 (MPI-ESM1. 2) and its response to increasing CO₂. *Journal of Advances in Modeling Earth*
706 *Systems*, 11(4), 998–1038.

707 Moreno, P. I., Videla, J., Valero-Garc es, B., Alloway, B. v, & Heusser, L. E. (2018). A continuous record of
708 vegetation, fire-regime and climatic changes in northwestern Patagonia spanning the last 25,000 years.
709 *Quaternary Science Reviews*, 198, 15–36.

710 Pausas, J. G. (2015). Bark thickness and fire regime. *Functional Ecology*, 29(3), 315–327.

711 Pausas, J. G., & Keeley, J. E. (2021). Wildfires and global change. *Frontiers in Ecology and the Environment*,
712 19(7), 387–395.

713 Pausas, J. G., & Ribeiro, E. (2013). The global fire–productivity relationship. *Global Ecology and Biogeography*,
714 22(6), 728–736.

715 Pechony, O., & Shindell, D. T. (2010). Driving forces of global wildfires over the past millennium and the
716 forthcoming century. *Proceedings of the National Academy of Sciences*, 107(45), 19167-19170.

717 Peltier, W. R., Argus, D. F., & Drummond, R. (2015). Space geodesy constrains ice age terminal deglaciation:
718 The global ICE-6G_C (VM5a) model. *Journal of Geophysical Research: Solid Earth*, 120(1), 450–487.

719 Piao, S., Wang, X., Park, T., Chen, C., Lian, X. U., He, Y., Bjerke, J. W., Chen, A., Ciais, P., T ommervik, H.,
720 Nemani R.R. & Myneni R.B. (2020). Characteristics, drivers and feedbacks of global greening. *Nature*
721 *Reviews Earth & Environment*, 1(1), 14–27.

Formatted: Font: Italic

Formatted: Font: Italic

722 [Portenga, E. W., Rood, D. H., Bishop, P., & Bierman, P. R. \(2016\). A late Holocene onset of Aboriginal burning](#)
723 [in southeastern Australia. *Geology*, 44\(2\), 131–134.](#)

724 Power, M.J., Ortiz, N., Marlon, J., Bartlein, P.J., Harrison, S.P., Mayle, F., Ballouche, A., Bradshaw, R.,
725 Carcaillet, C., Cordova, C., Mooney, S., Moreno, P., Prentice, I.C., Thonicke, K., Tinner, W., Whitlock, C.,
726 Zhang, Y., Zhao, Y., Anderson, R.S., Beer, R., Behling, H., Briles, C., Brown, K., Brunelle A., Bush, M.,
727 Clark, J., Colombaroli, D., Chu, C. Q., Daniels, M., Dodson, J., Edwards, M.E., Fisinger, W., Gavin, D.G.,
728 Gobet, E., Hallett, D.J., Higuera, P., Horn, S., Inoue, J., Kaltenrieder, P., Kennedy, L., Kong, Z.C., Long,
729 C., Lynch, J., Lynch, B., McGlone, M., Meeks, S., Meyer, G., Minckley, T., Mohr, J., Noti, R., Pierce, J.,
730 Richard, P., Shuman, B.J., Takahara, H., Toney, J., Turney, C., Umbanhowar, C., Vandergoes, M.,
731 Vanniere, B., Vescovi, E., Walsh, M., Wang, X., Williams, N., Wilmshurst, J., & Zhang, J.H. (2008).
732 Changes in fire regimes since the Last Glacial Maximum: an assessment based on a global synthesis and
733 analysis of charcoal data. *Climate Dynamics*, 30(7), 887–907.

734 Rodrigues, M., Costafreda-Aumedes, S., Comas, C., & Vega-García, C. (2019). Spatial stratification of wildfire
735 drivers towards enhanced definition of large-fire regime zoning and fire seasons. *Science of the Total*
736 *Environment*, 689, 634–644.

737 Rogers, B. M., Balch, J. K., Goetz, S. J., Lehmann, C. E. R., & Turetsky, M. (2020). Focus on changing fire
738 regimes: interactions with climate, ecosystems, and society. *Environmental Research Letters*, 15(3),
739 030201.

740 Rowe, C., Wurster, C. M., Zwart, C., Brand, M., Hutley, L. B., Levchenko, V., & Bird, M. I. (2021). Vegetation
741 over the last glacial maximum at Girraween Lagoon, monsoonal northern Australia. *Quaternary Research*,
742 102, 39–52.

743 Ruan, Y., Mohtadi, M., Dupont, L. M., Hebbeln, D., van der Kaars, S., Hopmans, E. C., Schouten, S., Hyer, E. J.,
744 & Schefuß, E. (2020). Interaction of fire, vegetation, and climate in tropical ecosystems: A multiproxy study
745 over the past 22,000 years. *Global Biogeochemical Cycles*, 34(11), e2020GB006677.

746 Rubino, M., D’Onofrio, A., Seki, O., & Bendle, J. A. (2016). Ice-core records of biomass burning. *The*
747 *Anthropocene Review*, 3(2), 140–162.

748 Scheiter, S., Kumar, D., Corlett, R. T., Gaillard, C., Langan, L., Lapuz, R. S., Martens, C., Pfeiffer, M., &
749 Tomlinson, K. W. (2020). Climate change promotes transitions to tall evergreen vegetation in tropical Asia.
750 *Global Change Biology*, 26(9), 5106–5124.

751 Schertzer, E., Staver, A. C., & Levin, S. A. (2015). Implications of the spatial dynamics of fire spread for the
752 bistability of savanna and forest. *Journal of Mathematical Biology*, 70(1), 329–341.
753 <https://doi.org/10.1007/s00285-014-0757-z>

754 Sedano, F., & Randerson, J. T. (2014). Multi-scale influence of vapor pressure deficit on fire ignition and spread
755 in boreal forest ecosystems. *Biogeosciences*, 11(14), 3739–3755. <https://doi.org/10.5194/bg-11-3739-2014>

756 Sidorenko, D., Rackow, T., Jung, T., Semmler, T., Barbi, D., Danilov, S., Dethloff, K., Dorn, W., Fieg, K.,
757 Gößling, H. F., Handorf, D., Harig S., Hiller W., Juricke S., Losch M., Schröter J., Sein D.V. & Wang Q.
758 (2015). Towards multi-resolution global climate modeling with ECHAM6–FESOM. Part I: model
759 formulation and mean climate. *Climate Dynamics*, 44, 757–780.

760 Snitker, G., (2018). Identifying natural and anthropogenic drivers of prehistoric fire regimes through simulated
761 charcoal records. *Journal of Archaeological Science*, 95, 1–15.

Formatted: Font: Italic

762 Song, M., Dodson, J., Lu, F., Shi, G., & Yan, H. (2023). A continuous paleorecord of vegetation and
763 environmental change from Erxianyan Wetland over the past 60,000 years in central China.
764 *Palaeogeography, Palaeoclimatology, Palaeoecology*, 111399.

765 Song, Y., Jiao, W., Wang, J., & Wang, L. (2022). Increased global vegetation productivity despite rising
766 atmospheric dryness over the last two decades. *Earth's Future*, 10(7).
767 <https://doi.org/10.1029/2021EF002634>

768 Stocker, B. D., Wang, H., Smith, N. G., Harrison, S. P., Keenan, T. F., Sandoval, D., Davis, T., & Prentice, I. C.
769 (2020). P-model v1. 0: an optimality-based light use efficiency model for simulating ecosystem gross
770 primary production. *Geoscientific Model Development*, 13(3), 1545–1581.

771 [Tallavaara, M., Luoto, M., Korhonen, N., Järvinen, H. and Seppä, H., 2015. Human population dynamics in
772 Europe over the Last Glacial Maximum. *Proceedings of the National Academy of Sciences*, 112\(27\),
773 pp.8232-8237.](#)

774 Tierney, J. E., Zhu, J., King, J., Malevich, S. B., Hakim, G. J., & Poulsen, C. J. (2020). Glacial cooling and climate
775 sensitivity revisited. *Nature*, 584(7822), 569–573.

776 van der Sleen, P., Groenendijk, P., Vlam, M., Anten, N. P. R., Boom, A., Bongers, F., Pons, T. L., Terburg, G.,
777 & Zuidema, P. A. (2015). No growth stimulation of tropical trees by 150 years of CO₂ fertilization but
778 water-use efficiency increased. *Nature Geoscience*, 8(1), 24–28. <https://doi.org/10.1038/ngeo2313>

779 Wang, H., Prentice, I. C., Keenan, T. F., Davis, T. W., Wright, I. J., Cornwell, W. K., Evans, B. J., & Peng, C.
780 (2017). Towards a universal model for carbon dioxide uptake by plants. *Nature Plants*, 3(9), 734–741.

781 [Williams, A. N., Ulm, S., Cook, A. R., Langley, M. C., & Collard, M. \(2013\). Human refugia in Australia during
782 the Last Glacial Maximum and terminal Pleistocene: A geospatial analysis of the 25–12 ka Australian
783 archaeological record. *Journal of Archaeological Science*, 40\(12\), 4612–4625.](#)

784 [Williams A.P., Allen C.D., Macalady A.K., Griffin D., Woodhouse C.A., Meko D.M., Swetnam T.W., Rauscher
785 S.A., Seager R., Grissino-Mayer H.D., Dean J.S., Cook E.R., Gangodagamage C., Cai M. & McDowell
786 N.G. \(2013\). Temperature as a potent driver of regional forest drought stress and tree mortality. *Nature
787 Climate Change* 3: 292–297.](#)

Formatted: Font: Italic

Formatted: Indent: Left: 0 cm

Formatted: Font: Italic